Unlocking the potential of half-metallic Sr_{2}FeMoO_{6} films through controlled stoichiometry and double-perovskite ordering

Adam J. Hauser, Robert E. A. Williams, Rebecca A. Ricciardo, Arda Genc, Manisha Dixit,

Jeremy M. Lucy, Patrick M. Woodward, Hamish L. Fraser, and Fengyuan Yang

Unlocking the potential of half-metallic Sr_2FeMoO_6 films through controlled stoichiometry and double-perovskite ordering

Adam J. Hauser[1], Robert E. A. Williams[2], Rebecca A. Ricciardo[3], Arda Genc[2], Manisha Dixit[2], Jeremy M. Lucy[1], Patrick M. Woodward[3], Hamish L. Fraser[2], Fengyuan Yang[1,*]

[1]Department of Physics, The Ohio State University
[2]Department of Materials Science and Engineering, The Ohio State University
[3]Department of Chemistry, The Ohio State University

Abstract

Phase-pure, fully epitaxial Sr_2FeMoO_6 films with a high degree of Fe/Mo ordering have been fabricated using ultrahigh vacuum sputtering and verified by a variety of techniques. Through identifying and controlling critical factors, such as stoichiometry, phase purity, and double-perovskite ordering, that complicate the growth of Sr_2FeMoO_6 films, we demonstrate characteristics of high-quality Sr_2FeMoO_6 films that have not been shown before. Our results include the first report of distinct magnetic shape anisotropy and via scanning transmission electron microscopy, the first direct observation of clear Fe/Mo ordering within the double perovskite framework.

PACS numbers: 75.70.-i, 75.47.Lx, 68.37.-d, 81.15.-z

Half-metallic ferromagnets (HMFs) are desired materials for spin injection/detection in magnetoelectronic devices due to their 100% spin polarization. A number of HMFs have been predicted and discovered over the past three decades [1-8]. Unfortunately, all known HMF materials have limitations which hinder their application in real world devices. For example, the manganite perovskites (e.g. $La_{2/3}Sr_{1/3}MnO_3$) are limited by their low Curie temperatures (T_C) [5, 6], CrO_2 is a metastable phase that is difficult to incorporate in devices [6], and Fe_3O_4 suffers from its poor conductivity [6, 7]. Double perovskites (DP) [8, 9] are among the most promising HMFs for room-temperature applications because of their high T_C (up to 725 K) [10] and the fact that they belong to a large family of isostructural compounds, which allows for the growth of complex epitaxial heterostructures. The challenge with double perovskites, as well as Heusler alloys [11], both of which are more chemically complex than other HMFs, is controlling the stoichiometry, defects, and chemical site ordering.

The report of half-metallicity in bulk Sr_2FeMoO_6 [8] with a T_C of 420 K and ideal saturation magnetization (M_S) of 4 μ_B per formula unit (f.u.) [12] motivated numerous studies in fabrication of epitaxial films of Sr_2FeMoO_6, using pulsed laser deposition (PLD) and sputtering [13-26]. However, it has proven challenging to grow Sr_2FeMoO_6 films that are stoichiometric, phase pure, fully epitaxial and exhibit a high degree of Fe/Mo ordering. These challenges explain the absence of reports of Sr_2FeMoO_6-based magnetic tunnel junctions (MTJs) that show a tunneling magnetoresistance (TMR) commensurate with the high spin polarization of the material [16, 23]. In fact, many of the Sr_2FeMoO_6 films reported in the literature are accompanied by impurity phases. Furthermore, the stoichiometry of Sr_2FeMoO_6 films has been largely ignored despite the fact that studies of bulk samples have shown that Sr_2FeMoO_6 is not a line compound with a fixed composition, but rather can vary from $Sr_2Mo_2O_6$ ($SrMoO_3$) to

2

$Sr_2Fe_{1.33}Mo_{0.67}O_6$ [27]. This non-stoichiometry arises because the oxidation state of molybdenum can readily change from +4 to +6, as well as the fact that Fe and Mo ions have similar sizes.

In this article, we used ultrahigh vacuum (UHV) magnetron sputtering to examine how changes in deposition conditions impact the stoichiometry, phase purity and magnetic properties of Sr_2FeMoO_6 epitaxial films. This comprehensive study has enabled us to obtain phase-pure Sr_2FeMoO_6 epitaxial films with a high degree of Fe/Mo ordering which was quantitatively probed with both X-ray diffraction (XRD) and aberration-corrected high-angle annular dark field (HAADF) scanning transmission electron microscopy (STEM) [17]. Films grown in this study show clear shape anisotropy between the in-plane and out-of-plane magnetizations, indicative of strong magnetic coupling throughout the film. Most importantly this study reveals the critical factors that dictate stoichiometry, phase purity, and Fe/Mo ordering in Sr_2FeMoO_6 films. Controlling these factors is the key to optimizing the magnetic properties, thereby unlocking the potential of Sr_2FeMoO_6 for use in magnetoelectronic devices.

Epitaxial Sr_2FeMoO_6 films were grown on $SrTiO_3$ (001) and (111) substrates in an UHV sputtering system with a base pressure of 5×10^{-10} Torr. Stoichiometric Sr_2FeMoO_6 targets were synthesized via multi-step chemical processing and sintering in forming gas (5% H_2 in N_2) using $SrCO_3$, Fe_2O_3, and MoO_3 as starting materials. XRD verified that the Sr_2FeMoO_6 targets are pure DP phase using a Bruker D8 Advance diffractometer in a Bragg-Brentano geometry. Direct-current (DC) magnetron sputtering was used for film deposition with a constant current of 5 mA or 100 mA. Ultra-pure Ar gas (99.9995%) was further purified by a Matheson NanoChem Purifilter to achieve a specified impurity level of one part per billion before entering the chamber for sputtering at pressures ranging from 6.7 to 300 mTorr. H_2 and O_2 with concentration down to 0.02% in Ar were also used in order to find the optimal reducing/inert/oxidizing environment for

Sr_2FeMoO_6 film growth. For most films discussed in this article, horizontal sputter sources and standard 90º off-axis geometry were used for deposition with the substrates positioned at a horizontal distance of 6.5 cm from the target and 9.0 cm below the center of the target [28]. The substrate temperature was varied between room temperature and 900 °C and the optimal temperature was identified to be 800 °C. Conventional on-axis sputtering geometry was also used to deposit Sr_2FeMoO_6 films for comparison.

The stoichiometry of the Sr_2FeMoO_6 films was determined using both Rutherford Backscattering (RBS) and Energy Dispersive X-ray (EDX) spectroscopy. RBS measurements were carried out at the Rutgers University and analyzed using the SIMNRA program. The epitaxial quality of the Sr_2FeMoO_6 films was characterized by a Bruker D8 Discover high-resolution triple-axis X-ray diffractometer. Magnetic properties of the Sr_2FeMoO_6 films were measured by a Quantum Design superconducting quantum interference device (SQUID) magnetometer and a LakeShore vibrating sample magnetometer (VSM). Aberration-corrected HAADF STEM imaging using a FEI Titan 80-300 microscope with a spatial resolution of 0.7 Å was used to reveal the crystallinity and interface quality as well as the Fe/Mo ordering in our Sr_2FeMoO_6 films. A knowledge of the film thickness is critical in the calculation of M_S, and for the measurement we used a combination of four techniques: profilometry over a chemically etched step, RBS analysis, small-angle X-ray reflectometry (XRR), and direct observation from HAADF STEM images which permitted counting of the atomic columns across total film thickness (observed in cross section).

The foremost important factor for fabrication of epitaxial films of complex materials such as double perovskites is to the stoichiometry. It is well known that growing stoichiometric films of complex materials is quite challenging. However, despite the large amount of work published

in the field, the stoichiometry of Sr_2FeMoO_6 films has been largely ignored in the literature. Due to the significant influence of stoichiometry on the magnetic properties of Sr_2FeMoO_6 [27], we systematically characterize the stoichiometry of our Sr_2FeMoO_6 films as a function of sample position, sputtering gas pressure, inert/reducing/oxidizing environment, and substrate temperature using both RBS and EDX. Surprisingly, the sputtering gas pressure plays a dominant role in the stoichiometry of the films. It is generally believed that for deposition of complex oxide epitaxial films using magnetron sputtering, off-axis geometry with high sputtering gas pressure (typically above 100 mTorr) is needed to minimize energetic bombardment [28]. Previously, magnetron sputtering in H_2/Ar at a total pressure of 76 mTorr was used to deposit Sr_2FeMoO_6 films [20-24] and in only one study was the film stoichiometry characterized [21].

Fig. 1 shows the RBS and EDX spectra for Sr_2FeMoO_6 films grown in pure Ar using off-axis geometry at a total pressure P_{Ar} of 70 mTorr and 6.7 mTorr. At P_{Ar} = 70 mTorr, RBS (Fig. 1a) and EDX (Fig. 1c) give a Mo:Fe ratios of 1.43 and 1.48, respectively. Since the RBS analysis prefers film thickness of 100 to 300 nm for separation of the peaks of elements and EDX prefers films as thick as possible, the film thicknesses in Figure 1 are different. However, we have done numerous measurements for each technique and verified that the Fe:Mo ratios do not change with film thickness within the instrument resolutions. The Sr signal from the substrate makes it difficult to get an accurate measure of stoichiometry for Sr using either RBS or EDX. Nevertheless, both RBS and EDX suggest that the amount of Sr is roughly comparable to the sum of Fe and Mo for most of our Sr_2FeMoO_6 films. A systematic study of stoichiometry in bulk Sr_2FeMoO_6 by Topwal *et al*. indicates that the magnitude of this off-stoichiometry (~45% Mo rich) drastically lowers the magnetization (from 3.2 μ_B/f.u. for stoichiometric composition to

~2.1 μ_B/f.u. at 4.2 K) and T_C (from 380 K for stoichiometric composition to ~270 K) in Sr$_2$FeMoO$_6$ [27]. Although the saturation magnetization of 3.2 μ_B/f.u. in ref. 27 is not at optimal Fe/Mo ordering as compared to the value of 3.96 μ_B/f.u. for a close to perfectly ordered Sr$_2$FeMoO$_6$ [29], the systematic variation of stoichiometry in a series of samples synthesized at similar conditions demonstrates the significant effect of stoichiometry on the magnetization [27]. By decreasing the Ar pressure to 6.7 mTorr, the stoichiometry is significantly improved to Mo:Fe = 1.12 by RBS (Fig. 1b) and Mo:Fe = 1.13 by EDX (Fig. 1d), corresponding to a composition of approximately Sr$_2$Fe$_{0.94}$Mo$_{1.06}$O$_6$. At this level of non-stoichiometry, both M_S and T_C only decrease slightly compared with stoichiometric Sr$_2$FeMoO$_6$ [27]. We varied the Ar pressure from 6.7 mTorr up to 300 mTorr and found that the Sr$_2$FeMoO$_6$ films monotonically become more off-stoichiometric (Mo rich) with increasing pressure.

The roles of other deposition parameters on the stoichiometry of Sr$_2$FeMoO$_6$ films are as follows: (1) In addition to pure Ar, we explored H$_2$/Ar and O$_2$/Ar environments with the H$_2$/O$_2$ concentration ranging from 0.02% - 2%. Although the change in redox characteristics of the sputter gas is an important parameter for phase formation as discussed below, the cation stoichiometry of the films is not sensitive to the introduction of low levels of H$_2$ or O$_2$. (2) The substrate temperature was also explored and it was found to have little effect on the film stoichiometry over the range from room temperature to 900 °C. (3) In order to investigate the effect of sample position on film stoichiometry, we positioned the substrate at several locations between the off-axis position and on-axis position. At high gas pressure (e.g., 70 mTorr), the Sr$_2$FeMoO$_6$ films always have Mo:Fe ratios in excess of 1.40 regardless of the substrate position. At low pressures such as 6.7 mTorr, the magnetic quality deteriorated significantly as the substrates moved towards directly facing the target due to the increasing bombardment.

A possible mechanism for the dependence of stoichiometry on total pressure is the difference in scattering of Fe (atomic mass = 55.85 amu) and Mo (95.94 amu) atoms by Ar (39.95 amu), resulting in different spatial distribution of sputtered Fe and Mo atoms. At high pressures, the sputtered species experience more scattering, which magnifies the imbalance between Fe and Mo, leading to considerable off-stoichiometry in the Sr_2FeMoO_6 films. At low pressures, the atoms experience less scattering and arrive at the substrate in a ratio that more closely maintains the stoichiometry of the target.

Phase purity and epitaxial quality are essential for realizing half-metallicity in Sr_2FeMoO_6 films. Unlike other complex oxides, the synthesis of Sr_2FeMoO_6 requires either an inert or reducing environment [27, 29]. A slight oversupply of oxygen promotes the formation of impurity phases, most notably $SrMoO_4$ and FeO_x. We characterized our Sr_2FeMoO_6 films using XRD systems with both Bragg-Brentano geometry for detecting impurity phases and triple-axis geometry for measurement of epitaxy, as shown in Fig. 2. The sputtering gas pressure again plays a major role in the phase purity of the Sr_2FeMoO_6 films. When using pure Ar at $P_{Ar} < \sim 50$ mTorr, the films are phase-pure perovskites. Fig. 2a shows the θ/2θ scan of a Sr_2FeMoO_6 (001) film grown at $P_{Ar} = 6.7$ mTorr with only the (00l) peaks and a c-axis pseudocubic lattice constant $a_{pc} = 7.909$ Å. This is slightly larger than the bulk value of 7.894 Å [8], suggesting that the film may have a small degree of in-plane strain due to the 1% lattice mismatch with $SrTiO_3$.

X-ray diffraction measurements on a Sr_2FeMoO_6 (111) film grown at $P_{Ar} = 6.7$ mTorr in Fig. 2b reveals only the (hhh) peaks with $a_{pc} = 7.982$ Å. Both films are phase pure without any detectable impurity phases. In addition, the Sr_2FeMoO_6 (111) film exhibits a strong (111) peak which reflects the DP ordering of Fe and Mo. Using Rietveld refinements, we fit the θ/2θ scan of the Sr_2FeMoO_6 (111) film and extracted the DP ordering parameter $\xi = 0.854 \pm 0.024$, where $\xi =$

$2(g_{Fe} - 0.5)$, and g_{Fe} is the refined occupancy of Fe on the Fe-site in the DP structure [29]. At $\xi =$ 0.854, 92.7% of the Fe atoms are correctly ordered in a DP lattice. Given the estimated stoichiometry of $Sr_2Fe_{0.94}Mo_{1.06}O_6$ which allows a maximum $g_{Fe} = 0.94$ and $\xi = 0.88$, the Fe and Mo ions are within experimental error as fully ordered as can be realized for this stoichiometry.

Fig. 2c shows an example $\theta/2\theta$ scan of a Sr_2FeMoO_6 (001) film grown at $P_{Ar} = 70$ mTorr with impurity phases of $SrMoO_4$ and Fe_3O_4 as well as a non-epitaxial Sr_2FeMoO_6 (112) peak. $SrMoO_4$ is the most common impurity phase in Sr_2FeMoO_6 films reported in the literature and Fe_3O_4 has also been previously observed [13, 14, 18, 25, 26]. Sr_2FeMoO_6 requires a narrow window of oxygen supply to form the DP phase. If the conditions become too oxidizing, formation of the Mo^{6+} containing $SrMoO_4$ is strongly favored. As a result, Fe_3O_4 can sometimes form if there is not enough Mo to pair with Fe in order to form Sr_2FeMoO_6 and non-epitaxial Sr_2FeMoO_6 growth can occur. For Sr_2FeMoO_6 films grown at $P_{Ar} = 70$ mTorr the $SrMoO_4$ phase is always present whereas Fe_3O_4 and non-epitaxial Sr_2FeMoO_6 are often observed.

The difference in the phase purity of the Sr_2FeMoO_6 films grown at $P_{Ar} = 6.7$ mTorr and 70 mTorr is likely caused by two sources. First, the films made at $P_{Ar} = 70$ mTorr have ~45% excess Mo, in contrast to the more stoichiometric films made at 6.7 mTorr. This off-stoichiometry at higher pressures may have favored formation of the $SrMoO_4$ impurity phase. Secondly, the oxygen needed for film growth should come exclusively from the target, and the oxygen pressure build-up in the chamber from sputtered oxygen increases at higher pressures due to the correspondingly lower gas replenish rates. Consequently, growth at $P_{Ar} = 70$ mTorr may lead to oxygen partial pressures that are high enough to form $SrMoO_4$. To suppress $SrMoO_4$ formation, we used H_2 in Ar to grow Sr_2FeMoO_6 films at a total pressure of 70 mTorr [20 - 24]. Below 0.3% H_2 in Ar, the $SrMoO_4$ phase remains. Within a range of 0.3% – 2% H_2 in Ar, we

obtained phase-pure Sr_2FeMoO_6 films. However, as mentioned above, even the phase-pure films are severely non-stoichiometric with ~45% excess Mo and have poor magnetic properties, including M_S below 1 μ_B/f.u. at $T = 5$ K and T_C below 300 K. The addition of O_2 in Ar promotes the formation of $SrMoO_4$ across the whole pressure range, with a significant degradation of magnetization.

The Φ-scans of the (110) peaks of a Sr_2FeMoO_6 (001) film and the $SrTiO_3$ substrate shown in Fig. 2d confirms the epitaxial relationship between the film and $SrTiO_3$. Fig. 2e shows the rocking curve of the Sr_2FeMoO_6 (004) peak for a Sr_2FeMoO_6 (001) film. The full-width-at-half-maximum (FWHM) of 0.096° demonstrates the high uniformity of the Sr_2FeMoO_6 film. The small-angle X-ray reflectometry (XRR) scan (Fig. 1f) of a Sr_2FeMoO_6 film shows more than 15 diffraction peaks, indicating smooth film surface and a sharp Sr_2FeMoO_6/$SrTiO_3$ interface. From the spacing between peaks, the thickness of the film is calculated to be 110 nm.

Fig. 3a and 3b show the in-plane ($H \parallel$ film) and out-of-plane ($H \perp$ film) magnetic hysteresis loops of a phase-pure Sr_2FeMoO_6 (111) epitaxial film at $T = 5$ K and 293 K, respectively. The hysteresis loops at both $T = 5$ K and room temperature show a distinct shape anisotropy between $H \parallel$ film and $H \perp$ film. The hysteresis loops with $H \parallel$ film (easy axis) exhibit sharp reversal with square-like loops while those with $H \perp$ film (hard axis) have slanted loops. The magnetic shape anisotropy originates from the minimization of magnetostatic energy and exists in most ferromagnetic films. To the best of our knowledge, there has been no report of the expected magnetic shape anisotropy in Sr_2FeMoO_6 films. The lack of magnetic shape anisotropy of previously reported films is likely due to the fact that the films are comprised of isolated magnetic domains with lateral sizes comparable to or smaller than the film thickness. As a result, the magnetic behavior of the films is similar to an ensemble of decoupled magnetic

9

nanoparticles. Decoupling between magnetic domains could be attributed to impurity phases (e.g. $SrMoO_4$), non-magnetic defects (e.g., Fe/Mo antisite disorders), or non-stoichiometry. The clear magnetic shape anisotropy seen in Fig. 3 indicates strong magnetic coupling over a range much larger than the film thickness.

Studies of bulk samples have shown that both T_C and M_S are sensitive to non-stoichiometry [27]. In order to accurately measure the film thickness which is critical in determining M_S, we used a combination of profilometry, XRR (Fig. 2f), STEM (see Fig. 4 below), and RBS. The M_S of 2.6 μ_B/f.u. is in good agreement with bulk results for samples with similar stoichiometry (12% excess Mo which corresponds to $Sr_2Fe_{0.94}Mo_{1.06}O_6$) [27]. The $M \sim T$ curve in Fig. 3c shows a clean single ferromagnetic phase transition with a $T_C = 380$ K. The observation of a single transition is an indicator of magnetic homogeneity, a feature that is not always observed for Sr_2FeMoO_6 films.

The HAADF STEM image in Fig. 4a shows the sharp interface between a Sr_2FeMoO_6 (001) film and the $SrTiO_3$ substrate alongside a schematic drawing of a DP lattice. Fig. 4b presents direct observation of Fe/Mo ordering in a Sr_2FeMoO_6 (111) film by HAADF STEM along the $<1\bar{1}0>$ direction. When viewed along this direction of the DP lattice, each lattice site becomes a column of pure Sr, Fe, or Mo atoms (no mixtures). In this imaging mode the intensity of the image in each atomic column is proportional to the chemical average atomic number. Each atomic column can be identified as Sr, Fe, or Mo (O is essentially invisible in HAADF STEM mode in our instrument). The most evident feature in Fig. 4b is the bright Sr-Mo-Sr triplets separated by a darker Fe atomic column. An enlarged view of the triplets present in Fig. 4b is given in Fig. 4c with the Sr, Fe, and Mo atoms labeled to outline the clear DP ordering. A schematic drawing of the projection of the DP lattice along the $<1\bar{1}0>$ direction is shown in Fig.

4c, which matches well with the STEM image. To the best of our knowledge, this is the first direct observation of clear DP ordering in Sr_2FeMoO_6 by HAADF STEM [17].

In summary, we have grown phase-pure fully-epitaxial Sr_2FeMoO_6 films and characterized those films using a variety of techniques. RBS and EDX show that the stoichiometry of the Sr_2FeMoO_6 films depends sensitively on the system pressure, with severe off-stoichiometry (~45% Mo rich) at P_{Ar} = 70 mTorr and close to stoichiometric composition ($Sr_2Fe_{0.94}Mo_{1.06}O_6$) at P_{Ar} = 6.7 mTorr. These films showed a high degree of Fe/Mo ordering (ξ = 0.854 ± 0.024), complete epitaxy, a smooth surface and sharp interface with the underlying $SrTiO_3$ substrate, and strong magnetic shape anisotropy. The results presented here provide critical understanding of this intriguing material and represent an important step toward the goal of incorporating half-metals into room-temperature magnetoelectric devices.

References:

1. de Groot, R. A., Mueller, F. M., van Engen, P. G., & Buschow, K. H. J., New Class of Materials: Half-Metallic Ferromagnets. *Phys. Rev. Lett.* **50**, 2024-2027 (1983).

2. Schwarz, K., CrO_2 predicted as a half-metallic ferromagnet. *J. Phys. F* **16**, L211-L215 (1986).

3. Ji, Y., et al., Determination of the Spin Polarization of Half-Metallic CrO_2 by Point Contact Andreev Reflection. *Phys. Rev. Lett.* **86**, 5585-5588 (2001).

4. Yanase, A. & Siratori, K., Band Structure in the High Temperature Phase of Fe_3O_4. *J. Phys. Soc. Jpn.* **53**, 312-317 (1984).

5. Pickett, W. E. & Singh, D. J., Electronic Structure and Half-Metallic Transport in the $La_{1-x}Ca_xMnO_3$ System. *Phys. Rev. B* **53**, 1146-1160 (1996).

6. Bibes, M. & Barthélémy, A., Oxide Spintronics. *IEEE Trans. Electron Devices* **54**, 1003-1023 (2007).

7. Brabers, V. A. M., Progress in spinel ferrite research. *Ferromagnetic Materials*, Vol. 8, edited by Buschow, K. H. J. (Elsevier, Amsterdam,1995) p. 189.

8. Kobayashi, K. L., Kimura, T., Sawada, H., Terakura, K., & Tokura, Y., Room-Temperature Magnetoresistance in an Oxide Material with an Ordered Double-Perovskite Structure. *Nature* **395**, 677-680 (1998).

9. Serrate, D., DeTeresa, J. M., & Ibarra, M. R., Double Perovskites with Ferromagnetism above Room Temperature. *J. Phys. Cond. Matter* **19**, 023201 (2007).

10. Krockenberger, Y., et al., Sr_2CrOsO_6: End Point of a Spin-Polarized Metal-Insulator transition by $5d$ Band Filling. *Phys. Rev. B* **75**, 020404(R) (2007).

11. Miura, Y., Nagao, K., & Shirai, M., Atomic disorder effects on half-metallicity of the full-Heusler alloys $Co_2Cr_{1-x}Fe_xAl$: A first-principles study. *Phys. Rev. B* **69**, 144413 (2004).

12. Sleight A.W. & Weiher J. F., Magnetic and electrical properties of $Ba_2M ReO_6$ ordered perovskites. *J. Phys. Chem. Solids* **33**, 679-687 (1972).

13. Manako, T., et al., Epitaxial thin films of ordered double perovskite Sr_2FeMoO_6. *Appl. Phys. Lett.* **74**, 2215-2217 (1999).

14. Yin, H. Q., Intra- versus intergranular low-field magnetoresistance of Sr_2FeMoO_6 thin films. *Appl. Phys. Lett.* **75**, 2812-2814 (1999).

15. Westerburg, W., Reisinger, D., & Jakob, G., Epitaxy and magnetotransport of Sr_2FeMoO_6 thin films. *Phys. Rev. B* **62**, R767-R770 (2000).

16. Bibes, M., et al., Tunnel magnetoresistance in nanojunctions based on Sr_2FeMoO_6. *Appl. Phys. Lett.* **83**, 2629-2631 (2003).

17. Wang, S. Q., Pan, H. Y., Zhang, X. P., Lian, G. J., & Xiong, G. C., Double-perovskite Sr_2FeMoO_6 epitaxial films with ordered cation structure grown in mixture gas of hydrogen and argon. *Appl. Phys. Lett.* **88**, 121912 (2006).

18. Sanchez, D., Garcia-Hernandez, M., Auth, N., & Jakob, G., Structural, magnetic, and transport properties of high-quality epitaxial Sr_2FeMoO_6 thin films prepared by pulsed laser deposition. *J. Appl. Phys.* **96**, 2736-2742 (2004).

19. Fix, T., et al., Pressure effect on the magnetization of Sr_2FeMoO_6 thin films grown by pulsed laser deposition. *J. Appl. Phys.* **97**, 024907 (2005).

20. Osugi, M., Asano, H., Hidashida, D., & Matsui, M., Magnetic Properties of Sputter-deposited Sr_2FeMoO_6 Thin Films. *J. Magn. Soc. Jpn.* **25**, 887-890 (2001) [in Japanese].

21. Asano, H., Osugi, M., Kohara, Y., Higashida, D., & Matsui, M., Room-temperature magnetic and magneto-optical properties of Sr_2FeMoO_6 thin films. *Jpn. J. Appl. Phys.* **40**, 4883-4885 (2001).

22. Asano, H., Kohara, Y., & Matsui, M., Coherent epitaxy and magnetic properties of Sr_2FeMoO_6 thin films on $Ba_{0.4}Sr_{0.6}TiO_3$-buffered $SrTiO_3$ substrates. *Jpn. J. Appl. Phys.* **41**, L1081-L1083 (2002).

23. Asano, H., Koduka, N., Imaeda, K., Sugiyama, M., & Matsui, M., Magnetic and junction properties of half-metallic double-perovskite thin films. *IEEE Trans. Magn.* **41**, 2811-2813 (2005).

24. Asano, H., Koduka, N., Takahashi, Y., & Matsui, M., XPS study of ferrimagnetic double perovskite thin films. *J. Magn. Magn. Mater.* **310**, 2174-2176 (2007).

25. Venimadhav, A., Sher, F., Attfield, J. P., & Blamire, M. G., Oxygen assisted deposition of Sr_2FeMoO_6 thin films on $SrTiO_3$(100). *J. Magn. Magn. Mater.* **269**, 101-105 (2004).

26. Jalili, H., Heinig, N. F., & Leung, K. T., X-ray photoemission study of Sr_2FeMoO_6 and $SrMoO_4$ films epitaxially grown on MgO(001): Near-surface chemical-state composition analysis. *Phys. Rev. B* **79**, 174427 (2009).

27. Topwal, D., Sarma, D. D., Kato, H., Tokura, Y., & Avignon, M., Structural and magnetic properties of $Sr_2Fe_{1+x}Mo_{1-x}O_6$ ($-1 \leq x \leq 0.25$). *Phys. Rev. B* **73**, 094419 (2006).

28. Eom, C. B., et al., Insitu grown $YBa_2Cu_3O_{7-\delta}$ thin-films from single-target magnetron sputtering. *Appl. Phys. Lett.* **55**, 595-597 (1989).

29. Huang, Y. H., Karppinen, M., Yamauchi, H., & Goodenough, J. B., Systematic studies on effects of cationic ordering on structural and magnetic properties in Sr_2FeMoO_6. *Phys. Rev. B* **73**, 104408 (2006).

30. Hauser, A. J., et al., Characterization of electronic structure and defect states of thin epitaxial $BiFeO_3$ films by UV-visible absorption and cathodoluminescence spectroscopies. *Appl. Phys. Lett.* **92**, 222901 (2008).

31. Yang. F. Y., et al., Uniaxial anisotropy and switching behavior in epitaxial CrO_2 films. *Appl. Phys. Let.* **77**, 286-288 (2000).

Figure Captions

Figure 1. RBS spectra of Sr_2FeMoO_6 films deposited on $SrTiO_3$ substrates in pure Ar (a) at P_{Ar} = 70 mTorr showing Mo:Fe ratio of 1.43, and (b) at P_{Ar} = 6.7 mTorr showing Mo:Fe = 1.12. EDX spectra of Sr_2FeMoO_6 films on $SrTiO_3$ give (c) Mo:Fe = 1.48 for P_{Ar} = 70 mTorr and (d) Mo:Fe = 1.13 for P_{Ar} = 6.7 mTorr.

Figure 2. $\theta/2\theta$ XRD scans of (a) a Sr_2FeMoO_6 (001) and (b) a Sr_2FeMoO_6 (111) phase-pure epitaxial films deposited by sputtering in pure Ar of 6.7 mTorr. Rietveld refinements (red curve in (b)) gives a DP order parameter ξ = 0.854 ± 0.024. (c) $\theta/2\theta$ scan of a Sr_2FeMoO_6 (001) film grown in pure Ar at P_{Ar} = 70 mTorr shows impurity phases of $SrMoO_4$ and Fe_3O_4 as well as non-epitaxial peak of Sr_2FeMoO_6 (112). The broad "bump" between 2θ = 25° and 50° is due to the plastic XRD holder [30]. (d) Φ-scans of the (110) peaks at a tilt angle Ψ = 45° for a Sr_2FeMoO_6 (001) film demonstrate epitaxial relationship between the film and the $SrTiO_3$ substrate. (e) A rocking curve of the Sr_2FeMoO_6 (004) peak for a Sr_2FeMoO_6 (001) film gives a FWHM of 0.096°. (f) Small-angle X-ray reflectometry scan of a Sr_2FeMoO_6 (001) film gives multiple diffraction peaks and a film thickness of 110 nm.

Figure 3. In-plane (black) and out-of-plane (red) hysteresis loops at (a) T = 5 K and (b) T = 293 K of a 115-nm thick Sr_2FeMoO_6 (111) epitaxial film deposited in pure Ar of 6.7 mTorr. The small opening in the out-of-plane loop at T = 5 K in (a) is due to the misalignment of the sample in SQUID measurements, in which a few degrees off-perfect alignment can result in obvious change in the shape of the loop [31]. The clear anisotropy between $H \parallel$ film and $H \perp$ film indicates strong magnetic interaction throughout the film. (c) M vs. T curve gives a T_C = 380 K.

Figure 4. *Unfiltered* aberration-corrected HAADF STEM images of (a) a Sr_2FeMoO_6 (001) film grown on a $SrTiO_3$ (001) substrate with an atomically sharp interface (the schematic drawing shows the double-perovskite lattice with rock-salt (NaCl) ordering of Fe and Mo), (b) a Sr_2FeMoO_6 (111) epitaxial film on $SrTiO_3$ viewed along the $<1\bar{1}0>$ direction with bright "triplet" patterns indicative of atomic number contrast, and (c) an enlarged STEM image highlighting the triplets (dashed blue box), each of which is a bright Sr-Mo-Sr chain (due to their high atomic numbers) separated by a darker Fe atomic column (lighter). It clearly shows the Mo-Fe ordering (green chain) separated by a Sr chain (red dashed line). The schematic in (c) is the projection of the DP lattice along the $<1\bar{1}0>$ direction, which matches the pattern seen in the STEM image of (c). The orientations in (c) are the same as in (b) indicated by the yellow axes.
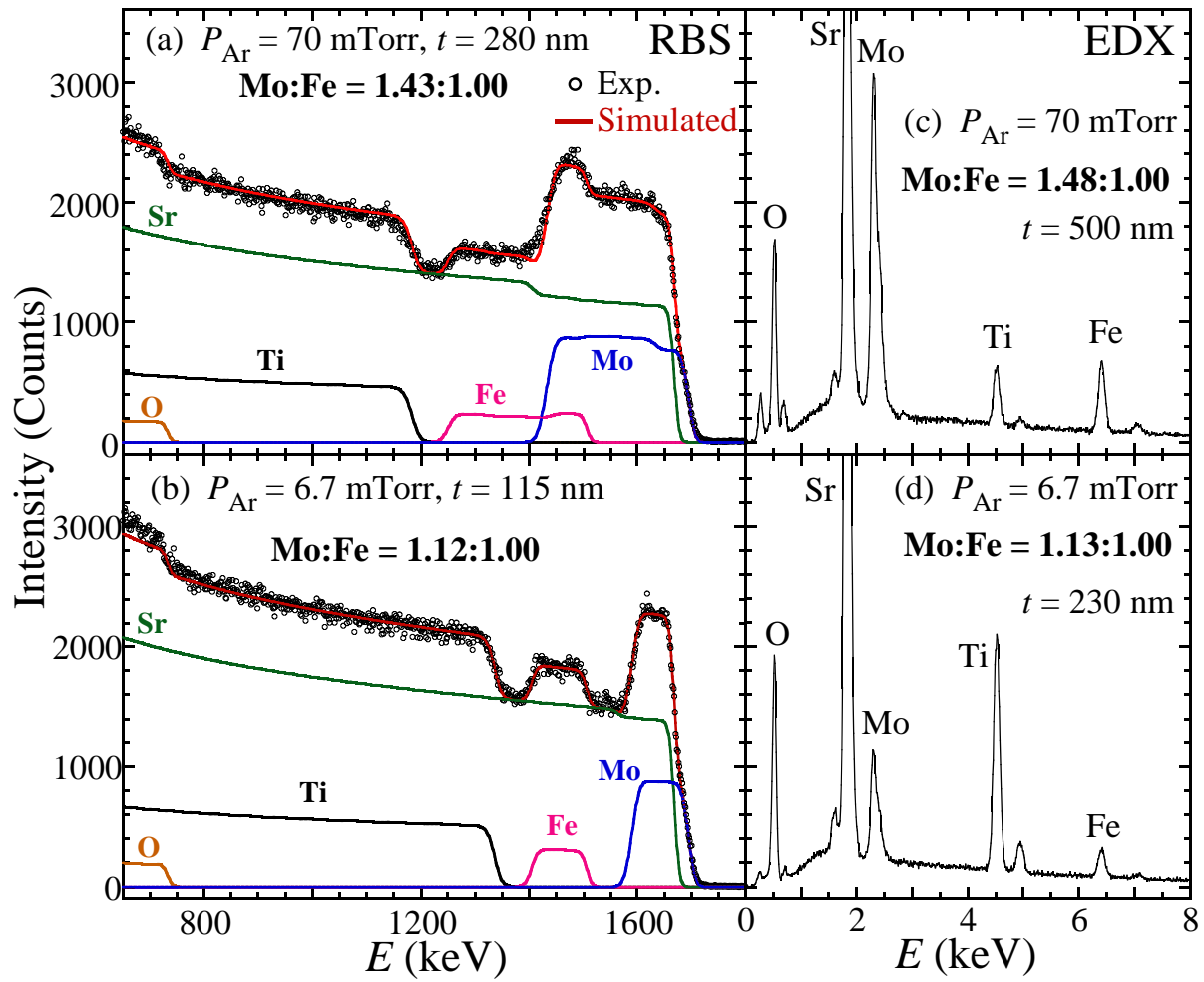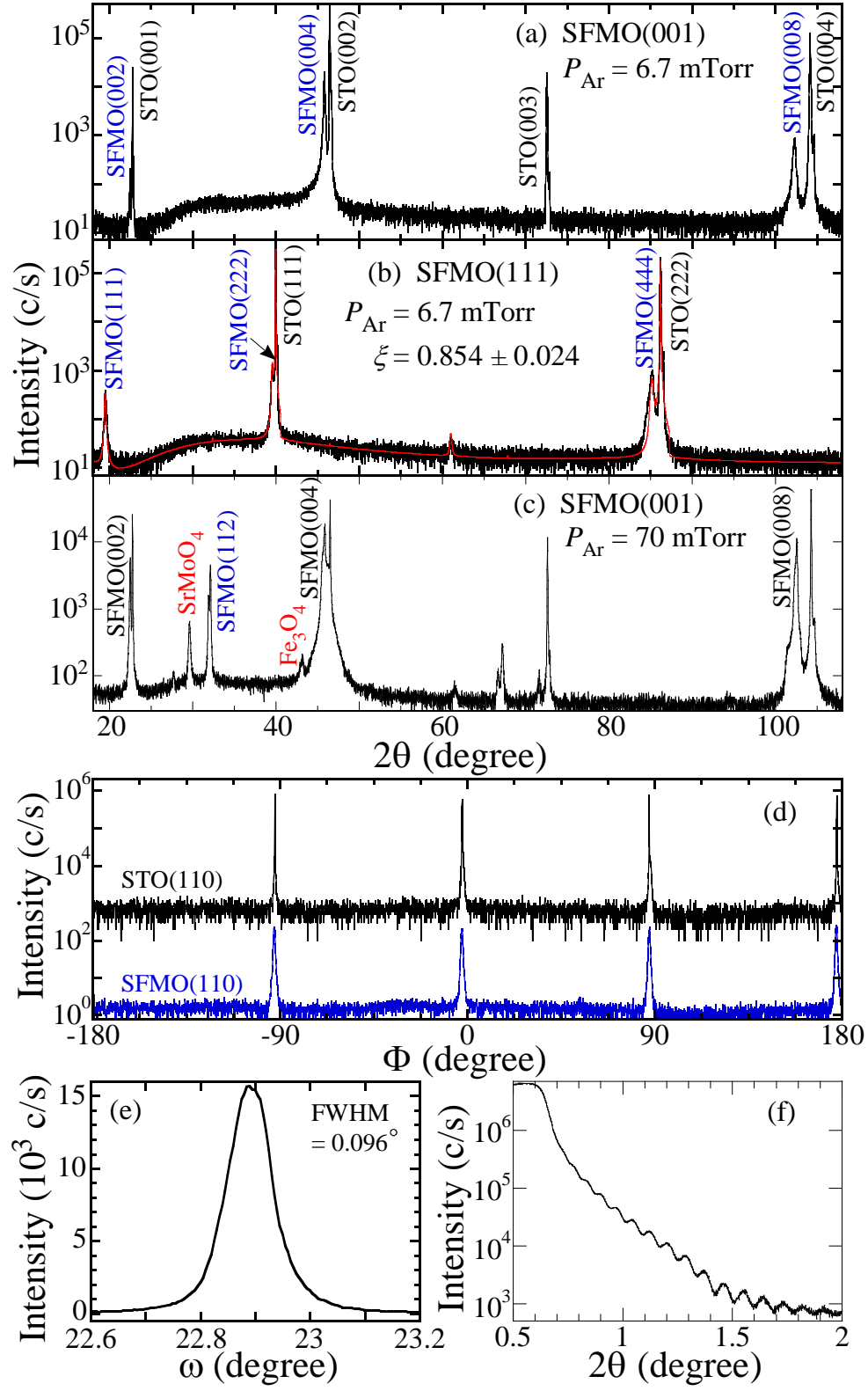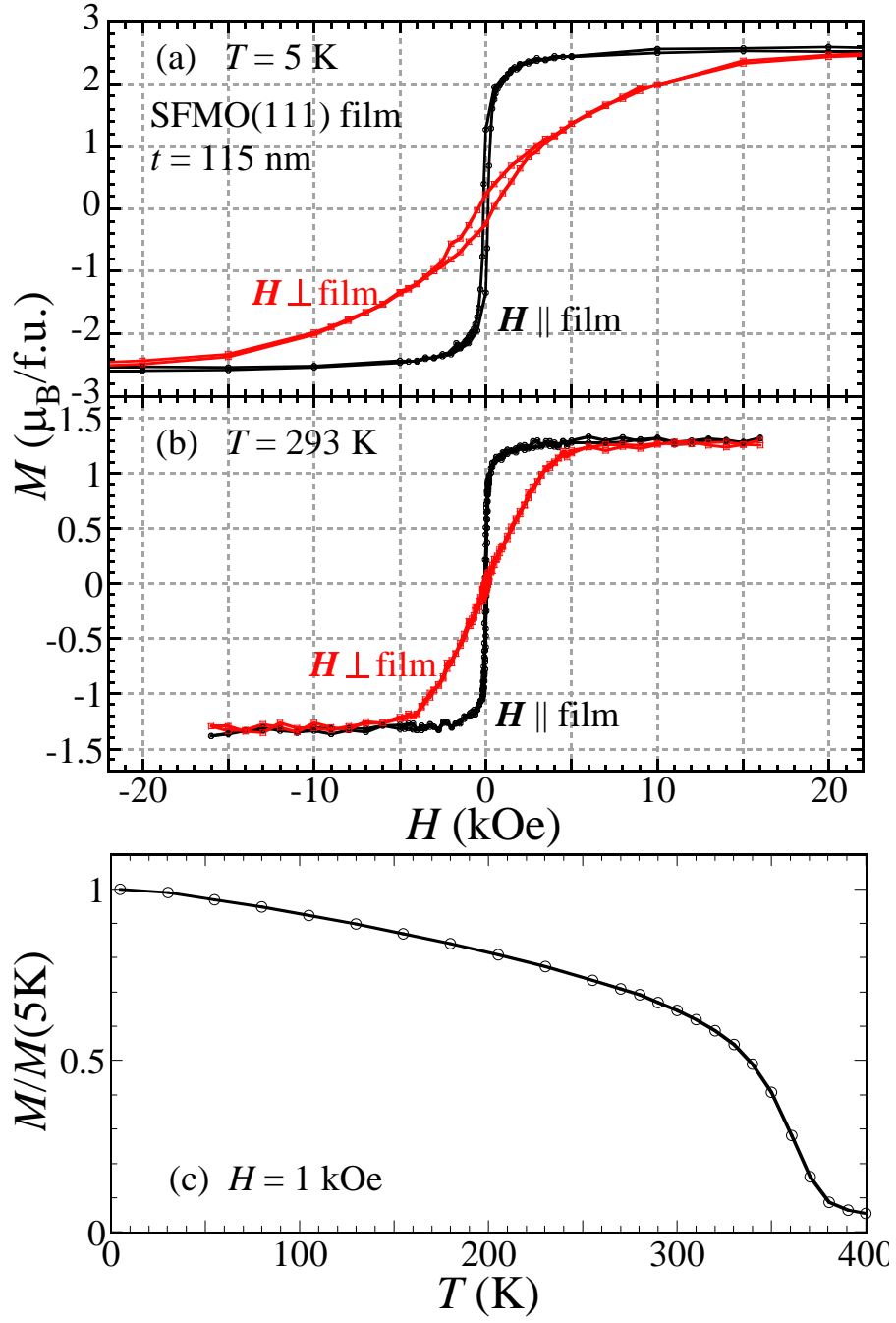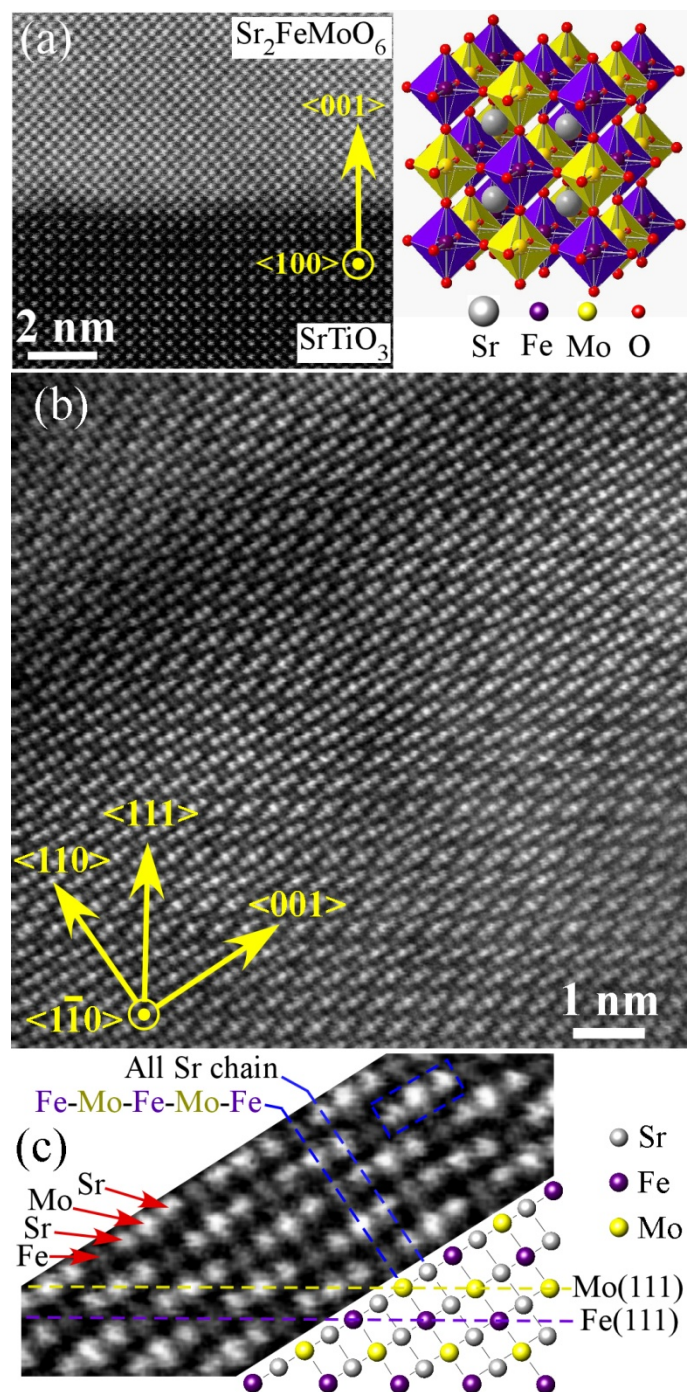
Fig. 1

Fig. 2

Fig. 3

Fig. 4